## Observation of hexatic liquid vortex matter in $YBa_2Cu_2O_{7-\delta}$

## Harald Hauglin

Department of Physics, University of Oslo, N-0316 Oslo, Norway
Nathan G. Woodard and Gregory P. Lafyatis

Department of Physics, The Ohio State University, Columbus, OH 43210-1106

(September 25, 2002.)

An atomic beam probe is used to study the structure and dynamics of quantized supercurrent vortex lines in YBa<sub>2</sub>Cu<sub>3</sub>O<sub>7- $\delta$ </sub> at temperatures up to within 0.7 K below  $T_C$ . Here we report the direct observation of a vortex configuration with sample wide bond-orientational order but only short range translational correlation. The data imply the existence of an intermediate 'hexatic' vortex line liquid phase. We find that the hexatic liquid is in thermal equilibrium over a narrow temperature range below  $T_C$  and is quenched into an immobile hexatic glass at low temperatures.

A magnetic field enters type II superconductors in the form of discrete supercurrent vortex lines, each carrying a quantum of magnetic flux. The microscopic structure and dynamics of vortex matter is not only crucial for the application of superconductors - since it limits the capacity for carrying electrical currents [1] - but also has a fundamental bearing on diverse topics such as the structure of liquid crystals [2] and the phase diagram of high density DNA mesophases [3]. In clean high- $T_C$  superconductors there is evidence for a first order melting transition from a low temperature rigid and crystalline vortex lattice to a high temperature mobile and disordered vortex liquid [4,5,6,7]. For the case of YBa<sub>2</sub>Cu<sub>3</sub>O<sub>7-d</sub>, there are indications that the melting transition changes character at critical points both at high  $(H_{ucp})$  [8,9] as well as low magnetic fields  $(H_{lcp})$  [10,11]. The interesting region of the vortex matter phase diagram just below  $T_C$  has previously proved inaccessible to vortex-

imaging-type studies and there are few detailed results on the microscopic structure of the vortex liquid.

In analogy with theories for 2D melting [12], it is predicted that extended line objects such as nematic liquid crystals [13] and quantized flux lines [14] can exhibit a hexatic line liquid phase with long range bond-orientational order but short range translational correlation. The experimental determination of a hexatic phase hinges on two issues: (i) the comparative range of translational and bond-orientational order and (ii) whether the structure is in thermal equilibrium. Early observations of hexatic correlations in the vortex array by low temperature decoration techniques [15,16] could not resolve whether the images represented a frozen-in vestige of a hexatic vortex liquid disordered due to thermal fluctuations or the ground state of a lattice disordered by static random pinning defects [17], such as found in charge density wave systems [18]. Decoration studies of BSCCO samples indirectly indicated an equilibrium hexatic structure significantly below  $T_C$  [19]. Recent Hall probe imaging of the vortex liquid phase in BSCCO [20] have been too limited to provide data on the range of correlations of the vortex liquid. Common to all these earlier reports is that they have probed a limited number of vortices ( $\lesssim 10^4$ ). We have used a new sensitive atomic beam technique to study directly vortex correlations in a high quality  $YBa_2Cu_3O_{7-\delta}$  single crystal in the low density regime below  $H_{lcp}$  for temperatures to within 0.7 K below  $T_C$ . We have probed correlations in a sample containing  $3 \times 10^5$  vortices, and report evidence for a hexatic vortex line liquid with sample wide bond-orientational order. We further demonstrate that the hexatic liquid is in thermal equilibrium over a narrow temperature range below  $T_C$  and is quenched into an immobile hexatic glass at low temperatures.

Experimentally, to probe vortex correlations, we pass a beam of potassium ( $^{39}$ K) atoms near the sample and detect magnetic resonance (MR) transitions driven by the microscopic magnetic field due to vortices (see Fig. 1a). Transitions are resonantly driven in atoms when the atomic velocity and the spacings of vortices along its path combine to make an oscillating magnetic field component at the magnetic resonance frequency  $f_0$ . We actually measure

the excitation probability for atoms as a function of their velocity and work backwards to infer spatial characteristics of the vortex array. If the atomic beam passes over an ordered vortex lattice, the MR transition will be strongly driven for velocities  $v = df_0$  corresponding to vortex row spacings d along the beam (fig 1b). Formally, to first order, the velocity dependent MR excitation probability,  $P_{\text{MR}}(v)$ , represents a projection of the vortex matter structure factor [21]:

$$P_{\text{MR}}(v) \sim \frac{1}{v^2} \int dq_y \left[ h(\mathbf{q}, z, \lambda) \right]^2 S_2(\mathbf{q}) , \quad q_x = 2\pi f_0 / v.$$
 (1)

Here  $h(\mathbf{q}, z, \lambda)$  is the Fourier transform of the field from a single vortex with penetration depth  $\lambda$  at height z above the surface [22] and  $\mathbf{q} = (q_x, q_y)$  is the in-plane wave vector. In analogy with x-ray scattering,  $[h(\mathbf{q}, z, \lambda)]^2$  may be identified as the vortex form factor, and, most importantly,  $S_2(\mathbf{q}) = \int \exp(-i\mathbf{q} \cdot \mathbf{r})g(\mathbf{r})d^2r$  is the 2D vortex lattice structure factor - the Fourier transform of the vortex pair distribution function  $g(\mathbf{r})$  [23]. Details on the experimental method are published elsewhere [21,24].

The experiments we report here were performed on a  $0.7 \times 1.7 \times 0.1 \text{ mm}^3 \text{ YBa}_2\text{Cu}_3\text{O}_{7-\delta}$  single crystal ( $T_C = 93.0 \text{ K}$ ,  $\Delta T_C < 0.3 \text{ K}$ ). The sample was grown by a self-flux method [25] and thermo-mechanically detwinned. Two electrical contacts ( $\leq 0.1\Omega$ ) are placed 1.3 mm apart on the top surface. The atomic beam skims the bottom surface along the a-axis and probes a  $0.7 \times 1.0 \text{ mm}^2$  area. A typical MR scan takes 30 s to acquire.

Figure 2 shows MR profiles recorded during cooling at a rate 0.2 K/min in a field 12 Oe parallel to the crystalline c-axis. We find that the MR profiles show two broad peaks for all temperatures  $T \leq 92.3$  K for which we detect a signal. Initially, upon cooling, there is a gradual screening of the magnetic flux from the sample. Below 90 K, the flux density is constant at 10.7 G, corresponding to a lattice constant  $a_0 \simeq 1.5 \,\mu\text{m}$ . This screening is seen as the slight increase of MR peak distances when the sample is cooled. The two peaks represent (projected) vortex row spacings for a vortex 'lattice' with a unit cell that is misaligned with respect to the atomic beam (similar to Fig. 1b, upper panel). In contrast, either an isotropic

vortex liquid or a 'powder pattern' of randomly oriented crystallites without sample wide orientational order would show a single bump representing the projection of a diffraction ring (Fig. 1b, bottom panel) [21,24]. An immediate conclusion is that the vortex array has sample wide orientational correlation in the entire temperature range probed.

A detailed analysis of the MR signal is necessary in order to extract the translational correlation length. The analysis is outlined here, details will be published elsewhere [21]. We model the atomic excitation using equation (1) and correct for saturation of the MR transition in a rate-equation approach [21]. Saturation is important since it broadens the MR peaks, especially when the magnetic field modulation is strong: close to the sample surface and at low temperatures (short penetration depth  $\lambda$ ). We model the vortex pair distribution function  $g(\mathbf{r}) = \sum_{l,m} f(\mathbf{r} - \mathbf{r}_{lm}, \sigma(r_{lm}))$ , where  $f(\mathbf{r}, \sigma) = (2\pi\sigma^2)^{-1} \exp(-r^2/2\sigma^2)$ and the sum runs over a lattice  $\mathbf{r}_{lm} = l\mathbf{r}_1 + m\mathbf{r}_2$  spanned by  $\mathbf{r}_1$  and  $\mathbf{r}_2$  (execpt l = m = 0). Orientational disorder is included by averaging the structure factor  $S_2(\mathbf{q})$  for a range of primitive lattice vectors  $\mathbf{r}_1$  and  $\mathbf{r}_2$  rotated over an angular interval of width  $\Delta\theta$ . The computed transition probability (1) is corrected for saturation and averaged over the relevant range  $z < 2 \mu m$  for direct comparison to the experimental data. The main model freedom is in the functional form of the displacement 'dispersion' function  $\sigma(r)$  and the orientational spread  $\Delta\theta$ . The unit cell parameters  $\mathbf{r}_1$  and  $\mathbf{r}_2$  are determined from the length scales for the two MR peaks, their relative intensities, and the flux density B, which is measured independently using a miniature Hall array.

The best fit to the experimental line shapes (smooth curves in Fig. 2) is for a triangular lattice that is tilted 18° with respect to the atom beam direction and compressed along that direction — the crystalline a-axis of the sample [26]. The fit is for a sample wide orientational disorder  $\Delta\theta \leq 2^{\circ}$ , a dispersion function of the form  $\sigma(r) = \sigma_0(r/a_0)^p$  with  $\sigma_0 = (0.14 \pm 0.01)a_0$  and roughness exponent  $p = 0.5 \mp 0.1$ . This dispersion implies a liquid-type short range order. The data could not be fitted using a quasi-long-range-order logarithmic dispersion predicted for the Bragg-glass phase [27]. The magnitude of the nearest

neighbor dispersion is consistent with the Lindeman criterion  $(\sigma_0/a_0 \sim 0.1 - 0.15)$  for a liquid near its melting point. Our experimental data therefore shows a vortex array with a liquid-like translational correlation length  $\xi_T = (16 \pm 8)a_0$  (determined by the criterion  $\sigma(\xi_T)/a_0 = 0.5$ ) that is much shorter than the orientational correlation length  $\xi_\theta \gg 500a_0$  (sample size).

Does this vortex pair distribution function represent a hexatic phase with true long range bond-orientational order [14] or does it reflect finite size effects in a vortex liquid with slowly decaying, yet short range, orientational order? Toner [28] argues that point defects affect translational order more than orientational order, and predicts that the correlation lengths should scale as  $\xi_{\theta} = \xi_T^2/a_0$  in the absence of orientational coupling with the underlying crystal. In this scenario, we would expect  $\xi_{\theta} < 10^3 a_0$ . We estimate a limit  $\xi_{\theta} > 10^5 a_0$  for the orientational correlation length by assuming that the angular disorder increases with distance as rapidly as the translational disorder, i.e.  $\Delta\theta(r) \sim (r/a_0)^{0.5}$ . Here  $\xi_{\theta}$  is defined by  $\Delta\theta(\xi_{\theta}) = 30^{\circ}$ . Clearly, this scaling is not satisfied – the orientational order is long ranged. The structural data in fig. 2 is therefore consistent with a hexatic vortex array with true long range orientational order. The absence of scaling is evidence that long range orientational order is induced by a coupling to the underlying crystal [29]. A further indication of this coupling is a preferred direction for the vortex array with respect to the crystalline axes [29]: we find repeated field cooling runs always produced vortex arrays with the same orientation.

Over which temperature range is the hexatic configuration in thermal equilibrium? The experiment shown in Fig. 3 addresses this issue. First, we observe that sample wide orientational order is destroyed by applying a strong current to the field cooled vortex array at 82 K. This is seen as the disappearance of the two distinct diffraction peaks for currents exceeding 220 mA (Fig. 3 a). (Note: 220 mA is almost an order of magnitude below the critical current for the sample at this temperature.) The broad MR line shape seen for large currents is consistent with a vortex array without sample wide orientational order. The stability of the disordered vortex array after the current is switched off (Fig. 3a, bottom curve) shows

that the transport current has introduced plastic deformations - the vortex array is not in thermal equilibrium at 82 K. Second, the sample is subsequently warmed and we observe the annealing of the disordered vortex array above 91 K (Fig. 3b); Specifically, we see the reappearance of the two distinct diffraction peaks - indicating long range bond-orientational order. This shows that the hexatic structure is in a thermal equilibrium (liquid) state over a  $\sim 2$  K interval below  $T_C$ .

For temperatures below 91 K the structure of the hexatic liquid is quenched into a hexatic glass. This happens when the dynamics of the vortex liquid and hence the evolution toward crystallization is stopped as thermal fluctuation energies become smaller than potential wells due to pinning centers. This scenario is supported by several experimental observations: (i) The minimum pinning energy is comparable to thermal energies at the glass formation temperature. The threshold current  $(I_{\min} = 120 - 220 \text{ mA} \text{ at } 82 \text{ K})$  for the onset of change in the vortex array structure (Fig. 3a), provides an estimate for the minimum vortex pinning force,  $F_{\rm min}=\phi_0I_{\rm min}/w\simeq5\times10^{-13}$  N. Here w=0.7 mm is the width of the sample. Assuming a quadratic pinning potential with a range comparable to the coherence length ( $\xi \sim 30 \text{ Å}$ ), the corresponding minimum threshold pinning energy is  $U_{\rm min}/k_B \simeq F_{\rm min}\xi/2k_B \sim 10^2 K$ . (ii) The amount of disorder does not change measurably between 90 K and 10 K. The best fit model comparisons (blue curves in Fig. 2) at 10 K and 91.5 K are for correlation functions  $g(\mathbf{r})$  with identical amount of disorder. The effect of temperature is included in the model line shapes only through the penetration depth dependence of the vortex form factor  $[h(\mathbf{q},z)]^2$  [22] in equation (1). The two curves are for  $\lambda_{ab}=140$  nm and 400 nm at 10 K and 91.5 K respectively.

Theoretically, the hexatic flux liquid should be bounded by two phase transitions [12,14]. At high temperatures, it should transform to an isotropic liquid by the proliferation of unbound disclinations. At low temperatures, the hexatic liquid should undergo a phase transition to a well ordered state (crystalline or Bragg glass [27]) by freezing out unbound dislocations. Our experimental data do not show any of these transitions. Assuming that

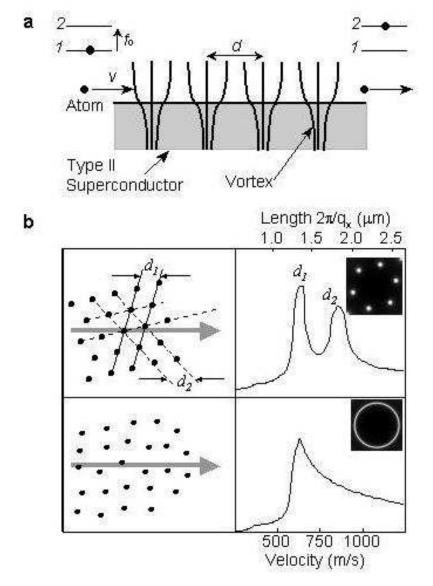
the hexatic-to-isotropic transition follows the established high field first order melting line [7,6,10], a simple extrapolation predicts  $T_m \simeq 0.9998T_C$  at 12 G – beyond the range of our method. On the low temperature side, we have shown that crystallization is preempted by the formation of a pinned hexatic vortex glass. The existence of a low density hexatic vortex liquid near  $T_C$  implies that the single first order melting transition for intermediate fields separate into two transitions in the region below the lower critical point  $H_{lcp}$ . The robustness of  $H_{lcp}$  with respect to oxygen vacancies and weak point defects due to electron irradiation [11], further suggests that a low field hexatic liquid phase could be a generic feature of the magnetic phase diagram of YBa<sub>2</sub>Cu<sub>3</sub>O<sub>7- $\delta$ </sub> below  $H_{lcp}$ . We believe that hexatic order is imposed on the vortex liquid due a coupling to the underlying electronic structure of the sample. The range of existence of hexatic phases in other high-T<sub>C</sub> materials may therefore depend on the anisotropy of the crystal structure.

- [1] For a review, see E. H. Brandt, Rep. Prog. Phys. 58, 1465 (1995).
- [2] C.-F. Chou, A. J. Jin, S. W. Hui, C. C. Huang, and J. T. Ho, Science **280**, 1424 (1998).
- [3] H. H. Strey et al., Phys. Rev. Lett. 84, 3105 (2000).
- [4] R. Cubitt et al., Nature **365**, 407 (1993).
- [5] E. Zeldov *et al.*, Nature **375**, 373 (1995).
- [6] M. Roulin, A. Junod, and E. Walker, Science **273**, 1210 (1996).
- [7] A. Schilling *et al.*, Nature **382**, 791 (1996).
- [8] M. Roulin *et al.*, Phys. Rev. Lett. **80**, 1722 (1998).
- [9] F. Bouquet et al., Nature **411**, 448 (2001).
- [10] M. Willemin *et al.*, Phys. Rev. Lett. **81**, 4236 (1998).

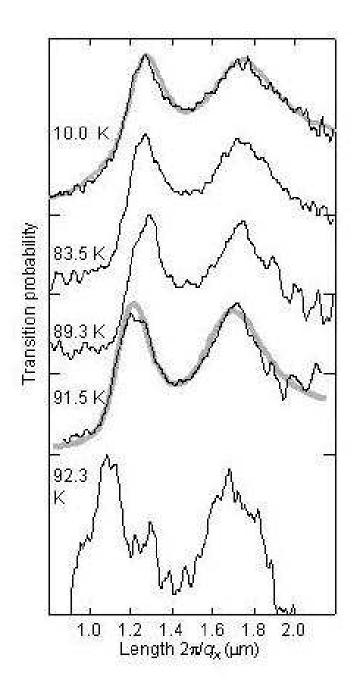
- [11] L. M. Paulius et al., Phys. Rev. B 61, R11910 (2000).
- [12] B. I. Halperin and D. R. Nelson, Phys. Rev. Lett. 41, 121 (1978); A. P. Young, Phys. Rev. B 19, 1855 (1979).
- [13] J. Toner, Phys. Rev. A 27, 1157 (1983).
- [14] M. C. Marchetti and D. R. Nelson, Phys. Rev. B 41, 1910 (1990)
- [15] C. A. Murray et al., Phys. Rev. Lett. **64**, 2312 (1990).
- [16] D. G. Grier. et al., Phys. Rev. Lett. 66, 2270 (1991).
- [17] E. M. Chudnovsky, Phys. Rev. B 40, 11355 (1989).
- [18] H. Dai and C. M. Lieber, Phys. Rev. Lett. 69 1576 (1992).
- [19] P. Kim, Z. Yao, and C. M. Lieber, Phys. Rev. Lett. 77, 5118 (1996).
- [20] A. Oral et al., Phys. Rev. Lett. 80, 3610 (1998).
- [21] H. Hauglin *et al.*, submitted to Phys Rev. B (available online at www.arXiv.org/cond-mat/0209150)
- [22] M. C. Marchetti, Physica C **200**, 155 (1992).
- [23] See e.g. J. M. Ziman, Models of Disorder, Cambridge University Press, 1979.
- [24] H. Hauglin, S. Dapore-Schwartz, N. G. Woodard, and G. P. Lafyatis, Physica C 235 240, 2697 (1994); S. Dapore-Schwartz, N. G. Woodard, and G. P. Lafyatis, Phys. Rev. B 55, 5655 (1997).
- [25] R. X. Liang et al., Physica C 195, 51 (1992).
- [26] This unit cell is similar to distorted vortex lattices reported by G. Dolan et al., Phys. Rev. Lett. 62, 2184 (1989).
- [27] T. Giamarchi and P. Le Doussal, Phys. Rev. Lett. 72, 1530 (1994).

- [28] J. Toner, Phys. Rev. Lett. **66**, 2523 (1991); J. Toner, Phys. Rev. Lett. **67**, 1810 (1991).
- [29] E. M. Chudnovsky, Phys. Rev. Lett. 67, 1809 (1991).
  - FIG. 1. (a) Experimental principle: The time dependent magnetic field seen by atoms moving near a sample with superconducting vortices drives magnetic resonance (MR) transitions in atoms. If the field has a strong Fourier component at the MR frequency  $f_0$ , then the transition  $1 \to 2$  will be strongly driven. For vortices spaced a distance d apart, the MR transition will be strongly driven for atoms moving with velocities near  $v = df_0$ . (b) Model predictions for two different vortex lattices. In both figures, the grey arrow indicates the direction of the atomic beam. For an ordered vortex lattice, the transition probability of the atoms, , has maxima at velocities corresponding to lattice row spacings along the beam. The upper example shows a 10.5 G hexatic lattice rotated 15 degrees with respect to the atomic beam similar to the case reported in this work. The two row spacings indicated,  $d_1$  and  $d_2$ , are readily identified with the two peaks in the data. Note: a triangular lattice with long range translational order would give a similar signal but with much taller and narrower peaks. For contrast, the lower example shows model predictions for 10.5 G isotropic liquid vortex structure. In reciprocal space, the signal corresponds to a projection of 2D vortex structure factor (shown in the insets) onto the beam direction.
  - FIG. 2. Atomic beam scans showing hexatic vortex matter structure. The MR transition probability versus length scale is measured during field cooling (at 0.2 K/min) in an applied field 12 Oe||c. The blue curves are best fit model predictions for identical structure factors with  $\lambda_{ab}$ = 140 and 400 nm at T=10 K and 91.5 K, repectively. The presence of two distinct MR peaks indicate sample wide orientational order. Note: the scale for each individual curve has been adjusted to fit on the graph. The signal strength at 10 K are 10 times larger than those at 91.5 K.
    - FIG. 3. MR profiles showing destruction of orientational order by a transport current

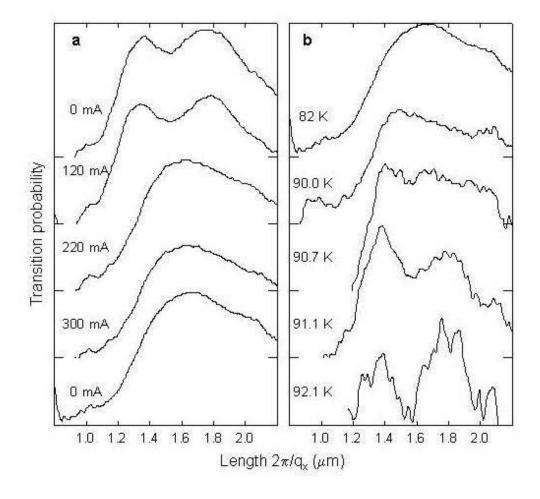
and subsequent restoration by annealing. (a) Current dependence of MR profiles. The sample was initially field cooled to 82 K in a 12 Oe field (top curve). MR transition profiles are shown for increasing currents (middle three curves). The bottom curve shows the MR profile 1 hour after turning off the 300 mA current. The broad bump at high current is due to a vortex array without long range order. (b) Annealing of the disordered vortex array. The top curve shows a MR profile due to the current induced disordered vortex array (panel a) after the current was turned off. The gradual appearance of two distinct peaks when annealing above 90 K shows the re-appearance of long range bond-orientational order.



H. Hauglin Figure 1



H.Hauglin Figure 2



H. Hauglin Fig 3